UCLA
UCLA Previously Published Works

Title
Extensive spontaneous plasticity of corticospinal projections after primate spinal cord injury.

Permalink
https://escholarship.org/uc/item/1t6846q5

Journal
Nature neuroscience, 13(12)

ISSN
1097-6256

Authors
Rosenzweig, Ephron S
Courtine, Gregoire
Jindrich, Devin L
et al.

Publication Date
2010-12-01

DOI
10.1038/nn.2691

Peer reviewed

Extensive Spontaneous Plasticity of Corticospinal Projections After Primate Spinal Cord Injury

Ephron S. Rosenzweig[1,*], **Gregoire Courtine**[2,3,*], **Devin L. Jindrich**[2], **John H. Brock**[1], **Adam R. Ferguson**[4], **Sarah C. Strand**[5], **Yvette S. Nout**[4], **Roland R. Roy**[2], **Darren M. Miller**[1], **Michael S. Beattie**[4], **Leif A. Havton**[2], **Jacqueline C. Bresnahan**[4], **V. Reggie Edgerton**[2], and **Mark H. Tuszynski**[1,6]

[1]Dept. of Neurosciences, University of California - San Diego, La Jolla, CA [2]Depts. of Physiological Science and Neurology, University of California, Los Angeles, CA [3]Dept. of Neurology, University of Zurich, Zurich, Switzerland [4]Dept. of Neurosurgery, University of California, San Francisco, CA [5]California National Primate Research Center, University of California, Davis, CA [6]Veterans Administration Medical Center, La Jolla, CA

Abstract

While axonal regeneration after CNS injury is limited, partial injury is frequently accompanied by extensive functional recovery. To investigate mechanisms underlying spontaneous recovery after incomplete spinal cord injury, adult rhesus monkeys underwent C7 spinal cord hemisections, with subsequent analysis of behavioral, electrophysiological and anatomical adaptations. We found remarkable spontaneous plasticity of corticospinal projections, with reconstitution of fully 60% of pre-lesion axon density arising from sprouting of spinal cord midline-crossing axons. This extensive anatomical recovery was associated with improvement in coordinated muscle recruitment, hand function and locomotion. These findings identify what may be the most extensive natural recovery of mammalian axonal projections after nervous system injury observed to date, highlighting an important role for primate models in translational disease research.

While the failure of extensive spontaneous regeneration of adult CNS axons contributes to limited recovery after clinically complete spinal cord injury (SCI), it has been recognized for some time that partial lesions to the mammalian spinal cord can be followed by remarkable and extensive recovery[1]. For example, monkeys and even humans subjected to spinal cord hemisection lesions that remove the lateral half of the spinal cord, including all corticospinal projections of that side, typically exhibit an extensive ability to recover volitionally guided locomotion[2–4]. While such recovery can be mediated in some mammals by spontaneous

plasticity of intraspinal circuitry5–6, primates require corticospinal projections for many features of fine voluntary movement7–8. These observations suggest that corticospinal axons may in fact exhibit a substantial capacity for intrinsic plasticity after adult CNS injury, despite a general consensus to the contrary9. To examine this hypothesis, we developed a primate model of C7 spinal cord hemisection to examine structural, electrophysiological and functional adaptations to the lesion at short (2 wk) and long (24 wk) time points after injury.

Fourteen naïve rhesus monkeys (*Macaca mulatta*) aged 5 –18 years (mean 9.6 ± 4.1 years; 13 male and 1 female) were divided into three groups of subjects. Group 1 (**Intact**): 3 intact subjects (including one female) underwent bilateral anterograde tracing of the corticospinal projections10, using different tracers in each hemisphere, and were sacrificed 7 weeks later. Group 2 (**Short-term lesion**): 4 monkeys underwent C7 lateral hemisection lesions and were sacrificed two weeks later; corticospinal projections were traced as in group 1, 7 weeks prior to sacrifice (i.e., 5 weeks prior to lesion). Group 3 (**Long-term lesion**): 7 monkeys underwent C7 lateral hemisection lesions and were sacrificed 4–8 months later; as in the other groups, corticospinal projections were traced 7 weeks prior to sacrifice. Lesion extent was assessed, and morphological responses of the corticospinal and raphespinal projections were identified caudal to the lesion site. Three of the long-term lesion subjects underwent chronic implantation of EMG electrodes into selected hindlimb and/or forelimb muscles. Recordings of electromyographic activity (n = 3) and kinematics (n = 5) during treadmill locomotion and skilled forelimb reaching were performed prior to spinal cord lesions and weekly thereafter (see Online Methods and Supplementary Table 1).

RESULTS

All hemisected subjects showed complete disruption of motor systems projecting through the right side of the spinal cord (Supp. Figs. 1 and 2). Notably, the lesion resulted in loss of detectable function in the right hand and leg immediately post-injury, associated with a failure to recruit most forelimb and hindlimb muscles (Figs. 1–3 and Supp. Fig 3). Locomotion and fine motor control with the left hand was unaffected (Supp. Fig. 4). While elbow movements rapidly recovered due to spared biceps motor pools11, right hand use was not detectable for at least 4 weeks post-lesion, despite significant levels of EMG activity in forelimb muscles. After this time, the hand exhibited spontaneous improvement in function, evidenced by partial recovery of ability to retrieve food rewards (raisins, grapes, and 1/12 apple pieces) from a flat surface (p<0.05, Fig. 1b,c). Substantial, well-timed recruitment of forelimb muscles, including motor pools innervating digit muscles, was detected during subsequent successful retrievals (Fig. 1a and Supp. Fig 3). Coordinated patterns of muscle recruitment associated with successful retrievals increased steadily after recovery onset (p<0.05, Fig. 1c) until a plateau (~60% of pre-lesion) was reached 12–16 weeks post-injury.

The ability to use the right forelimb (Fig. 2) and hindlimb (Fig. 3) during locomotion on a treadmill began to recover at the same time as fine motor control, i.e., 4–8 weeks post-lesion. Gait analysis at recovery onset showed that subjects with hemisections were not able to plantar step (Fig. 2a), had only limited weight bearing on the lesioned side as evidenced by reduced EMG activity in triceps and soleus muscles during stance (p < 0.01, Fig. 2f and Fig. 3a), and dragged the hindpaw during swing (p < 0.001, Fig. 3b). At 4–8 weeks post-

lesion, substantial co-activation of extensor and flexor motor pools innervating distal forelimb muscles was observed (Fig. 2a,e). From this time, locomotor capacities exhibited steady improvements; paw and hand antero-posterior placements converged towards pre-lesion values (p < 0.01, Fig. 2b and Fig. 3) and the variability of kinematic and limb endpoint trajectory significantly decreased (p < 0.01, Fig. 2c and Fig. 3c). Extensor muscles contributing to hindlimb and forelimb weight bearing recovered levels of EMG activity close to pre-lesion baseline, although significant differences nonetheless persisted (p<0.05, Fig. 2f). Recovery of the ability to reciprocally recruit extensor and flexor digit muscles (Fig. 2e) allowed subjects with hemisections to regain limited movements in distal forelimb extremities (p<0.05, Fig. 2). However, the amplitude (Fig. 2f) and temporal (Fig. 2a) patterns of EMG activity retained significant distinctions and impairments compared to intact animals, notably in distal flexor muscles (p < 0.01, Fig. 2f). There was a strong correlation between the recovery of forelimb and hindlimb locomotion as well as between the recovery of locomotion and fine motor control capacities (Supp. Fig 5). Subjects that recovered extensive forelimb use during stepping also regained the highest levels of skilled hand function during food retrieval.

Anatomical examination yielded an unexpected and remarkable degree of reconstitution of corticospinal tract axons below the lesion site at extended time points after injury (Fig. 4). Corticospinal projections arising from the left hemisphere were anterogradely labeled using 127 injections of dextran-conjugated alexa-488 (D-A488) into the left motor cortex, and projections from the right hemisphere were labeled with 127 similar injections of biotinylated dextran amine (BDA)10. Two weeks after C7 hemisection, the number of D-A488-labeled corticospinal axons (originating from the left hemisphere) in cervical spinal segments below the lesion site was reduced to $26 \pm 4\%$ of numbers observed in intact animals (Fig. 4). These remaining axons arise from unlesioned corticospinal projections that descend ipsilaterally, then decussate extensively across the primate (but not rodent) spinal cord midline10 (Supp. Fig. 1 and Fig. 4). By 24 weeks post-injury, the density of corticospinal axons was reconstituted to $60 \pm 9\%$ of values in intact monkeys, a spontaneous *2.3-fold* increase in axon density compared to early time points post-injury. This is likely an *underestimate* of the actual increase in corticospinal density, as Wallerian degeneration, which would clear the gray matter of all transected axons, was incomplete in the Short-term group (Supp. Fig. 6). The spontaneous increase in axon density was also observed among axons originating from the right (BDA-labeled) hemisphere which decussate at the pyramids, then re-cross the spinal cord midline (Fig. 4 and Supp. Fig. 7). While the density and caliber of corticospinal axons increased at extended time points post-lesion, qualitative analysis of their topographical distribution in gray matter did not show differences from intact subjects. There was no significant difference between Short-term and Long-term groups in the number of corticospinal axons decussating across the spinal cord midline (Supp. Fig. 8), suggesting that most of the increased corticospinal density in the Long-term group represents lesion-induced sprouting of axons that had already crossed the midline prior to the spinal cord lesion. This interpretation is further supported by serial reconstructions of axonal arbors, which reveal three phenomena suggestive of sprouting in the terminal arbors in lesioned subjects (Fig. 4k): a) higher densities of bouton-like swellings; b) small, thin processes, ending in swellings smaller than normal boutons; and c)

large axonal structures reminiscent of growth cones. Confocal microscopy revealed that these large structures bore synaptic elements, as they co-localized with synaptophysin (Fig. 4l–n). Additionally, corticospinal axons below the lesion level in Long-term subjects were significantly thicker than axons in Intact or Short-term lesion subjects (23% increase, p<0.05; Fig. 4 and Supp. Figs. 7 and 9), a phenomenon also observed in regenerating supernumerary motoneuronal axons12. Thus, primate corticospinal axons exhibit significant and substantial spontaneous plasticity after injury.

Comparison of corticospinal axon density at C5–6, above the injury, did not reveal significant differences among groups (p=0.4, Supp. Table 2).

Principal components analysis was used to assess the relationships among functional and anatomical responses to spinal hemisection in the Long-term group. Functional and anatomical data were aggregated, and eigenvalue decomposition of the correlation matrix among measures identified a large statistical cluster (PC1) that accounted for 59.2% of the total variance. Principal component loadings revealed that functional improvement of the affected forelimb during both locomotion and food retrieval from a platform was significantly associated with sprouting of corticospinal axons arising from both the left and right hemispheres (Fig. 5 and Supp. Fig. 10). The stability of this association was demonstrated with an iterative bootstrapping algorithm, whereby each subject was excluded in turn prior to PCA extraction. PC1 remained stable under these conditions (s = 0.75; r = 0.97; Supp. Fig. 10), demonstrating that the observed association between sprouting and functional recovery was not dependent solely on the data of one or two individual subjects. Rather, the sprouting-function association was present throughout the dataset, suggesting a robust relationship.

Immunolabeling for raphespinal axons was also performed to determine whether these systems, like corticospinal axons, exhibit spontaneous plasticity after spinal cord injury. Both Short-term and Long-term lesioned animals exhibited significantly fewer 5-hydroxytryptamine (5HT)-labeled axons on the lesion side compared to intact animals, and there was no increase in density over time post-lesion (Supp. Fig. 11).

DISCUSSION

The present study demonstrates a heretofore unidentified and substantial degree of spontaneous plasticity of corticospinal axons in the lesioned adult primate central nervous system that restores axon density to 60% of normal levels, and correlates with substantial improvements in both hand function and locomotion. These findings are consistent with electrophysiological measures showing extensive but uncoordinated muscle activity at early time points after lesions, likely arising from corticospinal axons decussating across the spinal cord midline, which become refined at subsequent time intervals to more coordinated patterns of muscle activity when corticospinal sprouting has occurred and function is improving.

Corticospinal axons are essential for dexterous volitional forelimb movement in primates7–8,13. Several features of spontaneous corticospinal axonal adaptation to injury in this

primate model are notable. First, rodents do not reconstitute the corticospinal system to this extent after injury. Rats reconstitute only 3% of total pre-lesion axon density when sprouting arises from the ventral corticospinal tract after dorsal column lesions14, or an estimated 5% when sprouting arises from the small population of midline decussating axons after pyramidotomy or spinal cord hemisection14–17. At the level of the *single* axon, rodent corticospinal axons may in fact exhibit an ability to sprout that equals the primate15–17; however, the differing neuroanatomical organization of the primate system allows a far greater proportion of all corticospinal axons to mount a sprouting response to the hemisection injury. That is, primate corticospinal axons extensively decussate across the spinal cord midline10,18, allowing reconstitution of 60% of pre-lesion axon density after C7 hemisection. Indeed, these midline-decussating axons exceed in total number those corticospinal axons that descend in the lateral and ventral columns, a feature of extensive corticospinal branching in primates10,18. In contrast, few corticospinal axons decussate across the rat spinal cord midline, resulting in a far smaller total magnitude of corticospinal axon density reconstitution in the rodent. Given the importance of corticospinal systems to voluntary movement in humans, and the extensive capacity of primate corticospinal axons to spontaneously sprout after injury, the translational relevance of rodent models to human outcomes might be improved by utilizing partial lesion models that spare a greater proportion of corticospinal axons, thereby allowing expression of greater total corticospinal plasticity in rodents. The remarkable 60% recovery in axon density at extended time points after injury in primates may be the most extensive recovery of axons described in the central nervous system to date. While other axonal systems in the central nervous system sprout in response to injury, including those of the hippocampus19, cortex20 and striatum21 following partial denervation, reconstitution of so high a proportion of original innervation has not, to our knowledge, been previously observed.

Second, the extensive spontaneous increase of corticospinal axon density after primate spinal cord hemisection identifies a mechanism potentially accounting for the remarkable recovery of function that can be observed after incomplete human SCI1,3–4. Humans sustaining spinal cord hemisection ("Brown-Sequard" syndrome) recover the ability to locomote and to partially use the affected hand3–4, as observed in our non-human primate model. Moreover, a second, more rostral hemisection on the opposite side of the spinal cord eliminates such recovery in both humans22 and non-human primates23, suggesting that the recovery depends on axons descending contralateral to the lesion. In contrast, rodents can exhibit basic locomotor function following such staggered, opposite side lateral hemisections of the thoracic spinal cord5. Under these circumstances, *de novo* intraspinal connections can relay the essential supraspinal information past the injury sites to restore hindlimb locomotion in mice and rats5–6. However, in contrast to the 50–70% recovery of skilled hand function reported here in non-human primates, cervical hemisections permanently abolish the ability of rats to retrieve food items with the hand24. Together, these data reinforce the viewpoint that the recovery of locomotion vs. fine motor function after incomplete SCI relies upon distinct neural mechanisms, and that the unique organization of the primate corticospinal system allows both humans and non-human primates to recover skilled hand function to a substantial extent. Indeed, humans with incomplete contusive traumatic spinal cord injury can exhibit extensive spontaneous

recovery: among humans with even slight sparing of motor and sensory function within 72 hours of spinal cord injury, 70% exhibit often substantial functional improvement when assessed 12 months later[1]. Corticospinal axons in primates are concentrated in dorsolateral white matter, with many axons located in the most superficial white matter of the spinal cord where sparing is most likely to occur after injury[25–26]. The retention of these corticospinal axons, and their spontaneous sprouting capability after injury, represents a compelling candidate mechanism for recovery in humans after incomplete human injury, and a potential substrate for improved recovery if this response can be enhanced therapeutically. Plasticity of other systems may also contribute to recovery: for example, disynaptic propriospinal projections can mediate dexterous finger movements in Rhesus monkeys after lesions of the dorsolateral cervical spinal cord[27–28]. Future studies will dissect the relative contributions to functional recovery of the corticospinal, propriospinal and other systems after SCI.

Third, the remarkable degree of spontaneous growth of *spared*, midline-decussating corticospinal axons in primates stands in distinct contrast to the inability of *transected* corticospinal axons to regenerate[9,29–30]. While the regeneration of a number of non-corticospinal motor systems such as rubrospinal, raphespinal and reticulospinal axons can be elicited in rodent models of SCI[9,31], elicitation of corticospinal regeneration using these same methods has not been demonstrated reliably. In separate and ongoing studies in this primate model, we fail to observe regeneration of transected corticospinal axons into cell grafts secreting the growth factors BDNF and NT-3 placed into the C7 hemisection lesion site[32]. Thus, there is a marked distinction in the ability of an intact corticospinal axon to sprout after spinal cord injury compared to the failure of a transected corticospinal axon to regenerate. Accordingly, future studies in both primates and rodents must identify cellular mechanisms underlying the spontaneous growth of intact corticospinal axons after spinal cord injury, allowing potential application of these mechanisms to therapeutically *enhance* spontaneous sprouting or induce *regeneration* of transected axons. This direction of research will be critical in generating therapies for humans with clinically complete spinal cord injury.

METHODS

Subjects

Fourteen naïve rhesus monkeys (Macaca mulatta) aged 5 –18 years (mean 9.6 ± 4.1 years; 13 male and 1 female) were studied. No effects of age were observed on any of the variables reported herein. All surgical and experimental procedures in these experiments were carried out using the principles outlined by Laboratory Animal Care (National Institutes of Health Publication 85-23, revised 1985) and were approved by the Institutional Animal Care and Use Committee (IACUC). Each animal was trained for a minimum of one month to perform quadrupedal treadmill locomotion and fine motor control tasks prior to surgeries.

Implantation of EMG electrodes

Monkeys were implanted with bipolar intramuscular EMG electrodes (Konigsberg Instruments, Pasadena, CA, USA) into selected muscles under aseptic conditions, as previously described[2]. Six muscles in the forelimb or hindlimb and forelimb of each

monkey received implants. The following muscles were selected: soleus, tibialis anterior, long head of the biceps brachii, medial head of the triceps brachii, pronator teres, flexor pollicis brevis profundus, flexor digitorum profundus, and extensor digitorum communis. Wound healing was monitored closely.

Lesion surgery

Animals were sedated with 1 mg/kg ketamine intramuscularly, anesthetized with 1.5–2.5% isoflurane, and the caudal half of the C5 dorsal lamina and the entire C6 dorsal lamina were removed. The dura was slit longitudinally along the midline and retracted gently. A surgical micro-knife was mounted on a stereotaxic arm, positioned at the spinal midline and midway between the C5 and C6 dorsal laminae. This rostrocaudal position corresponds to the C7 spinal cord segment. The stereotaxic manipulator was used to lower the blade through the entire dorsoventral extent of the spinal cord, without severing the ventral artery. This initial cut established the medial position of the lesion. The lesion was then completed using microscissors under microscopic observation by the surgeon (M.H.T.) to ensure lesion completeness laterally and ventrally. Animals retained bowel, bladder, and autonomic function after SCI.

Treadmill training and recordings

The monkeys were trained to walk quadrupedally on a motor-driven treadmill at speeds of 0.45, 0.89, 1.34, and 1.79 m/s. A plexiglass enclosure was used to maintain the animal in position while allowing video recording of movements. Food items were used for positive reinforcement. After completion of training, 3-D video recordings (100 Hz) were made using 4 cameras (Basler Vision Technologies) oriented at 45° and 135° bilaterally with respect to the direction of locomotion. Reflective markers were attached to the shaved skin bilaterally overlying the following body landmarks: the greater trochanter, the knee joint, the malleolus, the 5th metatarsal, and the outside tip of the fifth digit; for the forelimb, the head of the humerus, the elbow joint, the distal head of the ulna, the metacarpo-phalangeal joint, and the outside tip of the third digit. SIMI motion capture software (SIMI Reality Motion Systems) was used to obtain 3-D coordinates of the markers. The body was modeled as an interconnected chain of rigid segments, and joint angles generated accordingly[2]. Radio-transmitted EMG signals (2000 Hz) were amplified, filtered (10–1000 Hz bandpass), stored, and synchronized off-line with kinematic data.

Locomotor data analysis

For each monkey and each day of testing, 10 successive step cycles were extracted for both hindlimbs and both forelimbs from a continuous sequence of locomotion on the treadmill. A total of 88 parameters for the hindlimbs, and 71 parameters for the forelimb were computed for each gait cycle according to methods previously used in monkeys[2] and rats[33]. These parameters provided detailed quantifications of gait timing, joint kinematics, interlimb coordination and limb endpoint trajectory. Moreover, onsets and ends of EMG bursts were manually identified from filtered and rectified signals. Amplitudes, durations, and timings of EMG bursts were then computed for each muscle and gait cycle. To evaluate co-activation between muscles, probability density distributions of normalized EMG amplitudes of specific pairs of muscles during continuous treadmill stepping sequences were generated as

described previously[33]. Principal component analysis (PCA) was used to assess the degree of locomotor recovery[33]. Briefly, PCA was applied on all data computed from all gait cycles recorded in all monkeys before the injury and after 6 months of recovery post-lesion. Averaged scores on PC1 and PC2 were then extracted for each limb, monkey, and session. The degree of functional recovery was measured as the difference between pre- and post-lesion locomotor scores.

Training and recording of fine motor control tasks

To examine manual dexterity, a skilled motor task thought to reflect the functional integrity of corticospinal projections to the hand musculature was used. Subjects were chair trained and their behavior was shaped over several subsequent sessions to retrieve food rewards of three sizes from a platform. The monkeys were presented either with a raisin (10 trials/session, 2 consecutive daily sessions per wk), a grape (10 trials/session, 2 consecutive daily sessions per wk), or a 1/24 apple slice (5 trials/session, 2 consecutive daily sessions per wk) and the number of successful food retrievals was recorded for each session. In parallel, kinematics and EMG activity underlying forelimb retrievals were recorded using the same equipment and methods described for locomotion.

Axonal tracing

Subjects underwent anterograde tracing of both corticospinal projections using different tracers as previously described[10]. Briefly, subjects were deeply anesthetized as reported above, and biotinylated dextran amine (BDA; 10% solution in H_2O; 10,000 molecular weight; 150 nl/site; Molecular Probes, Eugene, OR) was injected into 127 sites spanning the arm, trunk and leg regions of the right motor cortex. Dextran-conjugated Alexa488 (D-A488) was injected using the same methods and into the corresponding coordinates in the left motor cortex. Seven weeks later, subjects were deeply anesthetized and transcardially perfused with a 4% solution of paraformaldehyde[10].

Tissue processing

The spinal cord dura was removed, and the spinal cord was cut in the transverse plane into blocks 1–1.5 cm-long, using the nerve roots as a guide to spinal level. The block containing the lesion was sectioned in the horizontal plane on a freezing microtome set at 30 μm intervals. Analogous blocks were obtained from the intact animals. Blocks containing segments C3–C6 and C8–T2 were sectioned in the transverse plane on a freezing microtome set at 40 μm. Tissue sections were stored at −20°C in cryoprotectant (25% glycerin, 30% ethylene glycol in 0.5 M phosphate buffer). Lesion extent was assessed in every 24th 30-μm-thick horizontal section stained for Nissl substance.

Detection of Corticospinal tracers

Transverse sections from the tissue blocks immediately rostral and caudal to the lesion block (segments C3–C4 and C8–T1) were selected for analysis of corticospinal and 5-HT density. For each tissue block, three sections, approximately 480 μm apart, were processed to detect the either D-A488 that had been injected into the left motor cortex, the BDA that had been injected into the right motor cortex, or 5-HT (total of 9 sections per block per animal). All

sections were washed in 0.1 M Tris-buffered saline (TBS; pH 7.4) three times for 10 minutes. Endogenous peroxidase activity was reduced with 0.6% hydrogen peroxide in 100% methanol for 30 minutes. Sections were then rinsed three more times in TBS, and processed separately for BDA and D-A488.

For D-A488 detection, sections were blocked and permeabilized for one hour in normal goat serum (NGS) and Triton X-100 (5% NGS, 0.25% TX-100, in TBS), then incubated for two nights at 4° C in rabbit anti-A488 (Invitrogen, 1:5000 in TBS with 5% NGS, 0.25% TX-100). Sections were then rinsed three more times in TBS, and incubated for one hour at room temperature in goat anti-rabbit poly-HRP-conjugated secondary antibody (Chemicon, 1:10 in TBS with 5% NGS, 0.25% TX-100).

For BDA detection, sections were incubated at 4°C overnight in an avidin-biotinperoxidase complex solution (Vectastain ABC Elite Kit, Vector Labs; 1:111).

For 5-HT detection, sections were permeabilized for one hour in 0.25% TX-100 in TBS (TBS-X), and incubated overnight at 4° C in goat anti-5HT (Immunostar; 1:10,000 in TBS-X). After three TBS washes, sections were incubated for 1 hr at room temperature in rabbit anti-goat secondary antibody (Vector Labs; 1:200 in TBS-X). After three more washes, sections were incubated for 1 hr at room temperature in a `tertiary' antibody: goat anti-rabbit poly-HRP-conjugated antibody (Chemicon; 1:10 in TBS-X).

After several more rinses in TBS, all sections were placed in a solution of diaminobenzidine (DAB) and $NiCl_2$ for 3–15 minutes until a dark reaction product was observed. Following three final rinses in TBS, sections were mounted on gelatin-coated slides, air dried, dehydrated, cleared, and coverslipped.

Fluorescent immunolabeling and confocal microscopy

Tranverse sections were permeabilized in 100% methanol for 30 minutes at room temperature, washed in TBS, and blocked in 5% normal donkey serum (NDS) in TBS-X for 1 hour at room temperature. Sections were then incubated in rabbit anti-A488 (Invitrogen, 1:500) and mouse anti-synaptophysin (Millipore, 1:1,000) diluted in 5% NDS in TBS-X for 2 days at 4°C. Sections were washed with TBS and incubated in fluorophore-conjugated secondary antibodies: donkey anti-rabbit A488 and donkey anti-mouse A594 (Invitrogen, each 1:200) diluted in 5% NDS in TBS-X for 2 hours at RT. Sections were washed in TBS, mounted on slides, and coverslipped with Fluoromount G (Fisher Scientific). Images were acquired with a FV1000 confocal microscope (Olympus) using sequential scanning to ensure no bleedthrough. Final images are composites of stacks of 13 images in Fig. 4l (final thickness 6.5 μm), and stacks of 24 images (final thickness 12 μm) in Fig. 4m,n

Quantification of corticospinal axon density, caliber, midline-crossing, and 5-HT axon density

Image capture and manipulation were performed as described previously10.

For D-A488 quantification, the intermediate zone of the gray matter was photographed with a 20× objective. Two separate focal planes were photographed per section, 3 sections per

animal (n = 3 Intact, n = 4 Short-term, n = 6 Long-term). Labeled corticospinal axons were detected and quantified in ImageJ 1.41c (Wayne Rasband, National Institutes of Health, rsb.info.nih.gov/ij/) using the FeatureJ plugin (Erik Meijering, www.imagescience.org/meijering/software/featurej/index.html) and custom-written scripts and algorithms (E.S.R.). After axon detection, the resultant binary images were skeletonized, so that all axons were 1 pixel wide. Thus, the sum of pixels in the skeletonized images is proportional to the total length of axons in the image. In parallel, the area of each axon segment was quantified using a non-skeletonized version of the binary image. Axon caliber was determined by dividing the area of each axon segment by its length.

For BDA quantification, in 3 sections per animal the entire lesion-side gray matter was photographed with a 10× objective, and multiple images were assembled into a montage in Adobe Photoshop. Analyses were restricted to the gray matter.

In addition, the number of BDA-labeled or D-A488-labeled axons crossing the spinal cord midline was counted in each section. Quantification was performed on an Olympus BX60 microscope with an Olympus OLY-200 video camera, a motorized stage and stage controller (MAC2002-XYZ, Ludl Electronic Products), and StereoInvestigator software (MicroBrightfield). Under low magnification (4× objective), a dorsoventral line was drawn which bisected the gray matter at the central canal. The line extended from the dorsal border of the midline gray matter to the dorsal border of the ventral fissure. The tissue was then examined under higher magnification (20× objective), and labeled axons that intersected this line were designated midline-crossing axons.

For 5-HT quantification, StereoInvestigator was used to outline lateral motor pools under low magnification and generate optical fractionator sampling sites. With a 100× objective, intersections of 5-HT-labeled axons with the inclusion lines of these sampling sites were marked.

Partial serial reconstructions of some axons were performed as described previously10.

Statistics and Principal Components Analysis

Values are reported as mean ± SEM. Statistics were calculated with Matlab (www.mathworks.com). Non-parametric tests (Kruskal-Wallis) were used unless otherwise noted.

Principal components analysis (PCA) was used to evaluate, in a data-driven manner, whether clustering of sprouting and functional outcomes accounted for a significant proportion of the variance in the dataset. Datasets from EMG, kinematics, food-retrieval success, and anatomical measures were manually curated and combined into a single large dataset. Several data pre-processing steps were taken to enable comparisons among measures from different outcome modalities (e.g., food retrieval vs. locomotor kinematics) and between time-variant and cross-sectional measures (e.g., recovery of function vs. sprouting measures). The variance from locomotor kinematic measures was consolidated in preliminary PC scores (see `Locomotor data analysis', above) and loadings were ipsatized such that return to baseline was reflected as higher scores. Functional performance measures

were averaged over the recovery interval, thereby making them temporally equivalent to the histological outcomes, which themselves reflect an aggregate of tissue changes over the duration of the study. PCA was performed using SPSS v.17 advanced models with missing values analysis. Testing of statistical assumptions (normality, heterogeneity of variance) was performed in SIMCA-P+ v.12. Principal component (PC) extractions were performed by the correlation method, standardizing the scale of the different outcomes to a mean of 0 and a standard deviation of 1. PCs were retained using a sequence of standard criteria including the eigenvalue > 1 rule34, scree plot35, and factor over-determination36–38. Component loadings with absolute values greater than 0.40 were considered `significant' and used for interpretation. To check for influential outliers, we performed a bootstrapping procedure, iteratively dropping each subject in turn and then re-running the PC extractions. The loading matrices from these different bootstrapped PC extractions were averaged and the pooled pattern was compared to the original PCA using Cattell's salient similarity index (S)39. Significant similarity for PC1 loading was observed between the pooled bootstraps and the original PCA, S = 0.75, suggesting a stable association between the degree of sprouting and behavioral recovery.

Supplementary Material

Refer to Web version on PubMed Central for supplementary material.

ACKNOWLEDGMENTS

REFERENCES

1. Fawcett JW, et al. Guidelines for the conduct of clinical trials for spinal cord injury as developed by the ICCP panel: spontaneous recovery after spinal cord injury and statistical power needed for therapeutic clinical trials. Spinal Cord. 2007; 45:190–205. [PubMed: 17179973]

2. Courtine G, et al. Performance of locomotion and foot grasping following a unilateral thoracic corticospinal tract lesion in monkeys (Macaca mulatta). Brain. 2005; 128:2338–2358. [PubMed: 16049043]

3. Little JW, Halar E. Temporal course of motor recovery after Brown-Sequard spinal cord injuries. Paraplegia. 1985; 23:39–46. [PubMed: 3982846]

4. Roth EJ, Park T, Pang T, Yarkony GM, Lee MY. Traumatic cervical Brown-Sequard and Brown-Sequard-plus syndromes: the spectrum of presentations and outcomes. Paraplegia. 1991; 29:582–589. [PubMed: 1787982]

5. Courtine G, et al. Recovery of supraspinal control of stepping via indirect propriospinal relay connections after spinal cord injury. Nat. Med. 2008; 14:69–74. [PubMed: 18157143]

6. Bareyre FM, et al. The injured spinal cord spontaneously forms a new intraspinal circuit in adult rats. Nat. Neurosci. 2004; 7:269–277. [PubMed: 14966523]

7. Lawrence DG, Kuypers HG. The functional organization of the motor system in the monkey. I. The effects of bilateral pyramidal lesions. Brain. 1968; 91:1–14. [PubMed: 4966862]

8. Hepp-Reymond MC, Trouche E, Wiesendanger M. Effects of unilateral and bilateral pyramidotomy on a conditioned rapid precision grip in monkeys (Macaca fascicularis). Exp. Brain Res. 1974; 21:519–527. [PubMed: 4442500]

9. Blesch A, Tuszynski MH. Spinal cord injury: plasticity, regeneration and the challenge of translational drug development. Trends Neurosci. 2009; 32:41–47. [PubMed: 18977039]

10. Rosenzweig ES, et al. Extensive spinal decussation and bilateral termination of cervical corticospinal projections in rhesus monkeys. J. Comp. Neurol. 2009; 513:151–163. [PubMed: 19125408]

11. Jenny AB, Inukai J. Principles of motor organization of the monkey cervical spinal cord. J. Neurosci. 1983; 3:567–575. [PubMed: 6827309]

12. Havton L, Kellerth JO. Regeneration by supernumerary axons with synaptic terminals in spinal motoneurons of cats. Nature. 1987; 325:711–714. [PubMed: 3821862]

13. Courtine G, et al. Can experiments in nonhuman primates expedite the translation of treatments for spinal cord injury in humans? Nat. Med. 2007; 13:561–566. [PubMed: 17479102]

14. Weidner N, Ner A, Salimi N, Tuszynski MH. Spontaneous corticospinal axonal plasticity and functional recovery after adult central nervous system injury. Proc. Natl. Acad. Sci. U. S. A. 2001; 98:3513–3518. [PubMed: 11248109]

15. Brus-Ramer M, Carmel JB, Chakrabarty S, Martin JH. Electrical stimulation of spared corticospinal axons augments connections with ipsilateral spinal motor circuits after injury. J. Neurosci. 2007; 27:13793–13801. [PubMed: 18077691]

16. Ghosh A, et al. Functional and anatomical reorganization of the sensory-motor cortex after incomplete spinal cord injury in adult rats. J. Neurosci. 2009; 29:12210–12219. [PubMed: 19793979]

17. Maier IC, et al. Constraint-induced movement therapy in the adult rat after unilateral corticospinal tract injury. J. Neurosci. 2008; 28:9386–9403. [PubMed: 18799672]

18. Lacroix S, et al. Bilateral corticospinal projections arise from each motor cortex in the macaque monkey: a quantitative study. J. Comp. Neurol. 2004; 473:147–161. [PubMed: 15101086]

19. Raisman G. Neuronal plasticity in the septal nuclei of the adult rat. Brain Res. 1969; 14:25–48. [PubMed: 5783115]

20. Dancause N, et al. Extensive cortical rewiring after brain injury. J. Neurosci. 2005; 25:10167–10179. [PubMed: 16267224]

21. Reader TA, Dewar KM. Effects of denervation and hyperinnervation on dopamine and serotonin systems in the rat neostriatum: implications for human Parkinson's disease. Neurochem. Int. 1999; 34:1–21. [PubMed: 10100192]

22. Nathan PW, Smith MC. Effects of two unilateral cordotomies on the motility of the lower limbs. Brain. 1973; 96:471–494. [PubMed: 4517841]

23. Turner WA. On hemisection of the spinal cord. Brain. 1891; 14:496–522.

24. Anderson KD, Gunawan A, Steward O. Quantitative assessment of forelimb motor function after cervical spinal cord injury in rats: relationship to the corticospinal tract. Exp. Neurol. 2005; 194:161–174. [PubMed: 15899253]

25. Bunge RP, Puckett WR, Becerra JL, Marcillo A, Quencer RM. Observations on the pathology of human spinal cord injury. A review and classification of 22 new cases with details from a case of chronic cord compression with extensive focal demyelination. Adv. Neurol. 1993; 59:75–89. [PubMed: 8420126]

26. Kakulas BA. A review of the neuropathology of human spinal cord injury with emphasis on special features. J. Spinal Cord Med. 1999; 22:119–124. [PubMed: 10826269]

27. Isa T, Ohki Y, Alstermark B, Pettersson LG, Sasaki S. Direct and indirect cortico-motoneuronal pathways and control of hand/arm movements. Physiology. 2007; 22:145–152. [PubMed: 17420305]

28. Sasaki S, et al. Dexterous finger movements in primate without monosynaptic corticomotoneuronal excitation. J. Neurophysiol. 2004; 92:3142–3147. [PubMed: 15175371]

29. Steward O, Sharp K, Yee KM, Hofstadter M. A re-assessment of the effects of a Nogo-66 receptor antagonist on regenerative growth of axons and locomotor recovery after spinal cord injury in mice. Exp. Neurol. 2008; 209:446–468. [PubMed: 18234196]

30. Hollis ER 2nd, Lu P, Blesch A, Tuszynski MH. IGF-I gene delivery promotes corticospinal neuronal survival but not regeneration after adult CNS injury. Exp. Neurol. 2009; 215:53–59. [PubMed: 18938163]

31. Bradbury EJ, McMahon SB. Spinal cord repair strategies: why do they work? Nat. Rev. Neurosci. 2006; 7:644–653. [PubMed: 16858392]

32. Brock JH, et al. Local and remote growth factor effects after primate spinal cord injury. J. Neurosci. 2010; 30:9728–9737. [PubMed: 20660255]

33. Courtine G, et al. Transformation of nonfunctional spinal circuits into functional states after the loss of brain input. Nat. Neurosci. 2009; 12:1333–1342. [PubMed: 19767747]

34. Kaiser HF. The application of electronic computers to factor analysis. Ed. Psych. Meas. 1960; 20:141–151.

35. Cattell RB. The Scree Test For The Number Of Factors. Multivar. Behav. Res. 1966; 1:245–276.

36. Hogarty KY, Hines CV, Kromrey JD, Ferron JM, Mumford KR. The Quality of Factor Solutions in Exploratory Factor Analysis: The Influence of Sample Size, Communality, and Overdetermination. Ed. Psych. Meas. 2005; 65:202–226.

37. Guadagnoli E, Velicer WF. Relation of sample size to the stability of component patterns. Psychol. Bull. 1988; 103:265–275. [PubMed: 3363047]

38. MacCallum RC, Widaman KF, Zhang S, Hong S. Sample size in factor analysis. Psych. Methods. 1999; 4:84–99.

39. Cattell RB, Balcar KR, Horn JL, Nesselroade JR. Factor pattern matching procedures: An improvement of the S index; with tables. Ed. Psych. Meas. 1969; 29:781–792.
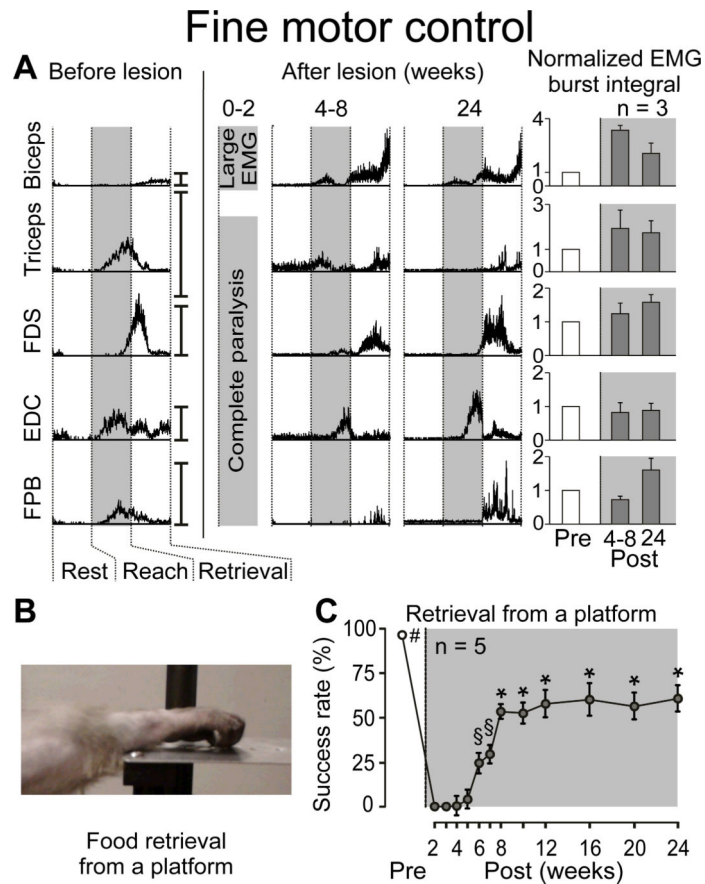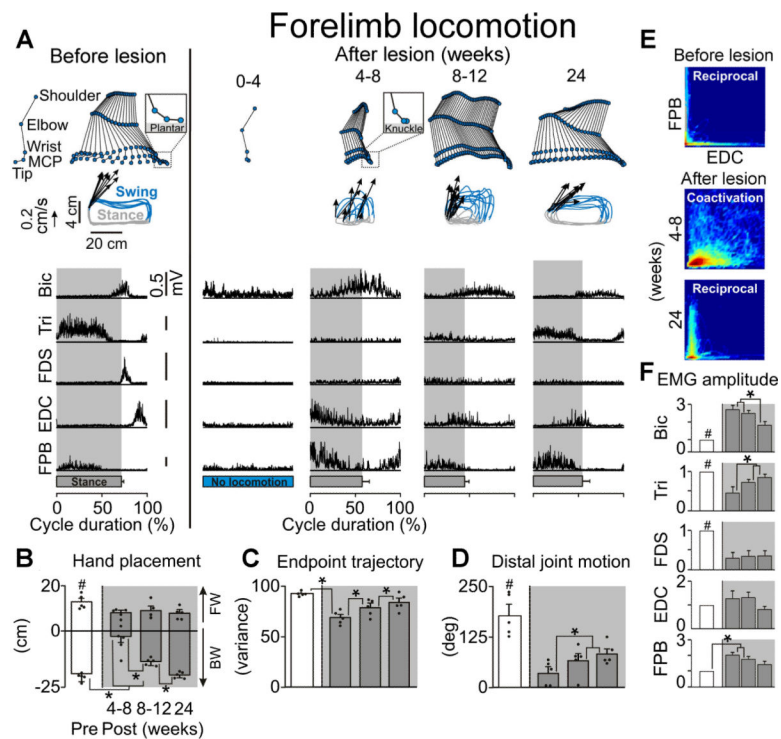
Figure 1. Spontaneous Improvement in Object Retrieval with the Hand After C7 Lateral Hemisection

A: Representative EMG activity recorded from forelimb muscles during successful retrievals before and after injury (10–15 trials per time point). Traces are normalized with respect to the timing of forelimb motion, i.e., rest, reach and retrieval, as indicated by vertical dotted lines. The reach phase corresponds to the time from the onset of forelimb motion to contact of the hand with the food item. The retrieval phase begins from the end of the reach phase and finishes with contact of the food item to the mouth. Vertical scale bars on the right side of each trace denote 100% of peak muscle activity during locomotion at 1 mph. Time points are shown as a range of weeks to emphasize inter-individual differences in the timing of the recovery. Mean integrated EMG amplitudes (+SEM) for forelimb EMG bursts during successful retrievals are shown. No statistical differences were detected in the amplitude of EMG burst amplitudes between pre- and post-lesion retrievals. **B**: Fine motor control task. From a standardized starting position, monkeys used their affected arm to retrieve a food item resting on a platform. **C**: Mean success in hand use reported as a percent of successful food retrieval trials (±SEM) in 5 monkeys. #, §, and * denote conditions that are significantly different (p<0.05) from all time points not marked with the same symbol. FDS, Flexor Digitorum Superficialis; EDC, Extensor Digitorum Communis; FPB, Flexor Pollicis Brevis.
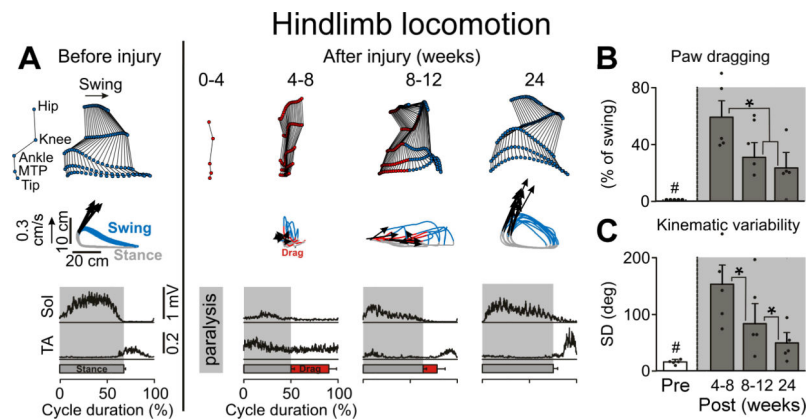
Figure 2. Partial Recovery in Forelimb Use During Locomotion After C7 Hemisection
A: Representative stick diagram decompositions (30 ms between sticks) of the right
(lesioned) forelimb motion during the swing phase while stepping quadrupedally on the
treadmill at 0.45 m/s before and at different time points post-injury. The successive (n=10
steps), color-coded trajectories of the forelimb endpoint (metacarpo-phalangeal joint, MCP)
are shown together with the intensity and direction of the forelimb endpoint velocity
(arrows) at swing onset. Mean (n=10 steps) integrated EMG activity of selected forelimb
muscles is represented for the different time points. The shaded area indicates the duration
of the stance phase. **B**: Mean (+SEM) values for the posterior (negative direction) and
anterior (positive direction) positions reached by the forelimb endpoint (MCP) with respect
to the shoulder (horizontal distance) during each gait cycle. Dots represent individual values
(n = 5 monkeys). **C**: Consistency of forelimb endpoint trajectory measured by principal
component analysis. Mean (+SEM) values of the amount of variance explained by the first
principal component are reported. **D**: Mean (+SEM) values for the amplitude of distal joint
motion measured during each gait cycle. **E**: Probability density distributions of normalized
EMG amplitudes in the flexor pollicis brevis (FPB) and extensor digitorum communis
(EDC) during treadmill stepping. L-shape pattern observed during stepping pre-lesion
indicates reciprocal activation between the antagonist FPB and EDC motor pools. D-shape
during stepping at 4–8 weeks post-lesion indicates co-activation between the FPB and EDC.
F: Mean EMG amplitude (+SEM) for forelimb EMG bursts during locomotion (n=3
monkeys). #, significantly different from all other time points at p<0.05; *, significantly
different from indicated time points at p<0.05.

Figure 3. Extensive Recovery of Hindlimb Locomotion After C7 Hemisection
A: Representative stick diagram decompositions (30 ms between sticks) of lesion-side hindlimb movements during the swing phase while stepping quadrupedally on the treadmill at 0.45 m/s before and at different time points post-injury. The successive (n = 10 steps), color-coded trajectories (blue, swing; red, drag; grey, stance) of the hindlimb endpoint (MTP) are shown together with the intensity and direction of the hindlimb endpoint velocities (arrows) at swing onset. Mean integrated EMG activity (n = 10 steps) of selected hindlimb muscles (Sol, Soleus; TA, Tibialis Anterior) is shown at the bottom of the panel for each time point. Shaded areas indicate the duration of the stance phase, red bars indicate the duration of paw dragging. **B**: Mean (+SEM) duration of paw dragging expressed as a percentage of the total swing phase duration at each time point tested. Dots represent individual values (n = 5). **C**: Mean (+SEM) variability of hip, knee, ankle, and MTP joint movements expressed as the sum of the standard deviation (SD) for each joint over 10 successive gait cycles. #, significantly different from all other time points at p<0.05. *, significantly different from indicated time points at p<0.05.

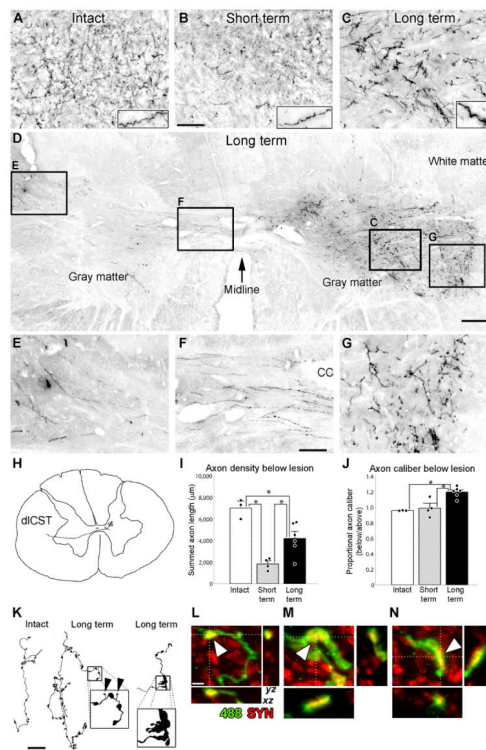**Figure 4. Extensive Compensatory Plasticity of the Lesioned Corticospinal Tract in Primates**
A–C: Compensatory sprouting of lesioned, D-A488-labeled corticospinal axons in the
intermediate zone of the gray matter caudal to the C7 hemisection. Insets demonstrate
increased axon caliber in Long-term subjects, quantified below. D–G: Corticospinal axons in
right-side gray matter below the lesion originate from the opposite (left) side of the spinal
cord. **D:** Long-term lesioned subject. Lesion is on right side; arrow denotes midline. Boxed
regions are shown at higher magnification. E–G demonstrate the path of corticospinal axons
as they (**E**) exit the left dorsolateral fasciculus, (**F**) decussate across the spinal cord midline
(cc, central canal), and (**G**) terminate in the lateral motor neuron pools. **H:** Serial
reconstruction of a single axon, demonstrating unequivocally that it originates from the left
dorsolateral corticospinal tract. **I:** Corticospinal axon density was reduced ~75% two weeks
after injury, and recovered to more than half of prelesion axon density by 24 weeks post-
lesion. **J:** Quantification of axon thickness. Long-term lesioned animals exhibited a 20%
increase in axon caliber below the lesion. There were no significant differences between
groups in axon density or caliber above the lesion level, therefore the observed changes were
not due to variability in tracer efficacy. In (I) and (J), dots denote individual animals' data
points, * indicate $p < 0.05$. **K:** Serial reconstructions of axonal arbors in an Intact (left) and
lesioned, Long-term (middle and right) subjects. Axons in lesioned, Long-term subjects
exhibit: i) high densities of bouton-like swellings (compare left and middle); ii) small, thin
processes, ending in swellings much smaller than normal boutons (middle inset,
arrowheads); and iii) large, abnormal structures that exhibit morphological features
resembling growth cones (right inset). **L–N:** Colocalization (arrowheads) of the synaptic
marker synaptophysin (red) with DA488-labeled (green) bouton-like swellings in axons
sprouting below the C7 lesion site in the Long-term group: **L** is a normal-appearing bouton-

like swelling, and **M, N** are examples from atypically large boutons found only in Long-term subjects as shown in panel **K**. Scale bar A–C, 100 μm; D, 250 μm; E–G, 86 μm; K, 25 μm; L–N, 2 μm. Error bars indicate SEM.
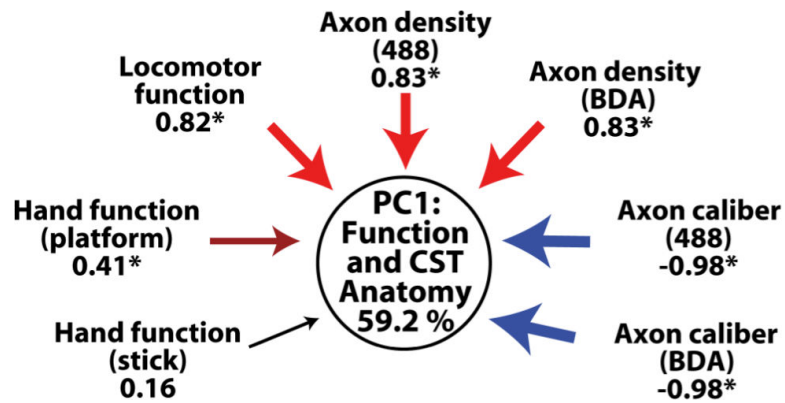
Figure 5. Relationship Between Anatomical Plasticity and Functional Recovery
Principal components analysis in the four Long-term subjects with both functional and anatomical data reveals a multivariate relationship between corticospinal sprouting density and functional recovery. The first principal component (PC1; circle) reflects a data-driven statistical clustering of the histological and functional outcome variables. Positive loading (analogous to a positive Pearson correlation) of variables onto PC1 is indicated in shades of red, and negative loading (analogous to an inverse Pearson correlation) is indicated in shades of blue. The magnitude of the loading is indicated by arrow thickness and below each variable; asterisks indicate statistical significance (|loading| > 0.40). Note that axon density co-loads on PC1 with both locomotor function on a treadmill and success in recovering food rewards from a platform. PC1 accounts for 59.2% of the variability in the data.